SIAM J. APPL. MATH.
Vol. 81, No. 2, pp. 574–590

© 2021 Society for Industrial and Applied Mathematics

Downloaded 05/01/21 to 131.111.184.3. Redistribution subject to SIAM license or copyright; see https://epubs.siam.org/page/terms

PREDICTING LIFT-OFF TIME WHEN DEEP-FRYING POTATO DOUGH SNACKS*

T. BABB†, G. P. BENHAM‡, J. BOWS§, R. GONZALEZ-FARINA†, K. B. KIRADJIEV†, W. T. LEE¶, AND S. TIBOS§

Abstract. When frying potato snacks, it is typically observed that the dough, which is submerged in hot oil, after some critical time increases its buoyancy and floats to the surface. The lift-off time is a useful metric in ensuring that the snacks are properly cooked. Here we propose a multiphase mathematical model for the frying of potato snacks, where water inside the dough is evaporated from both the top and bottom surfaces of the snack at two receding evaporation fronts. The vapor created at the top of the snack bubbles away to the surface, whereas the vapor released from the bottom surface forms a buoyant blanket layer. By asymptotic analysis, we show that the model simplifies to solving a one-dimensional Stefan problem in the snack coupled to a thin-film equation in the vapor blanket through a nonlinear boundary condition. Using our mathematical model, we predict the change in the snack density as a function of time and investigate how lift-off time depends on the different parameters of the problem.

Key words. multiphase, Stefan, asymptotic

AMS subject classifications. 80A22, 80A20, 35B40

DOI. 10.1137/19M1294253

1. Introduction. Frying is one of the oldest and most common forms of food cooking and has multiple functions, including to sterilize, dehydrate, and create product texture [1]. Generally there are two types of frying: shallow-fat frying and deep-fat frying. Here we focus on deep-fat frying in which the food product being cooked is fully immersed in the oil. During deep-fat frying, some food products undergo density changes that cause them to rise within the oil bath. This process can be exploited in food manufacturing, either as a way of determining the stage of cooking, or as a mechanism to collect the food from the hot oil. For example, in the production of potato snacks, uncooked snacks are submerged in hot oil by a conveyor belt and, as the dough cooks, they become buoyant and detach. Once the snack rises from the belt it interacts with a second submerged component. Knowing the lift-off duration is key to understanding when and where the snack interacts with the second submerged component. This interaction has product quality and fryer performance implications. This must happen at precisely the right moment in order to maximize product quality and the productivity of the process. To ensure that the snacks robustly detach at

*Received by the editors October 21, 2019; accepted for publication (in revised form) January 28, 2021; published electronically April 26, 2021.
https://doi.org/10.1137/19M1294253
Funding: This work was supported by PepsiCo. The work of the first, fourth, and fifth authors was supported by the EPSRC through grant EP/L015803/1.

†Mathematical Institute, University of Oxford, Andrew Wiles Building, Radcliffe Observatory Quarter, Woodstock Road, Oxford OX2 6GG, United Kingdom (Thomas.Babb@maths.ox.ac.uk, gonzalezfari@maths.ox.ac.uk, Kristian.Kiradjiev@maths.ox.ac.uk).

‡LadHyX, UMR CNRS 7646, Ecole polytechnique, 91128 Palaiseau, France, and Department of Earth Sciences, University of Cambridge, Bullard Laboratories, Madingley Road, Cambridge CB3 0EZ, UK (graham.benham@ladhyx.polytechnique.fr).

§PepsiCo International, 4 Leycroft Road, Leicester LE4 1ET, United Kingdom (John.Bows@pepsico.com, stacie.tibos@pepsico.com).

¶School of Computing and Engineering, University of Huddersfield, Queensgate, Huddersfield HD1 3DH, United Kingdom, and MACSI, Department of Mathematics and Statistics, University of Limerick, Limerick, Ireland (w.lee@hud.ac.uk).

Copyright © by SIAM. Unauthorized reproduction of this article is prohibited.

Downloaded 05/01/21 to 131.111.184.3. Redistribution subject to SIAM license or copyright; see https://epubs.siam.org/page/terms

the right time, a better quantitative understanding of the underlying mechanism is needed. In particular, there are two major contributions to buoyancy due to the generation of steam, which either escapes from the snack causing a reduction in density or becomes trapped underneath the snack in a vapor blanket.

Several different mathematical modeling approaches can be found within the food frying literature. For a comprehensive summary of all relevant types of models, see [13]. Many of these emphasise transport mechanisms of gases and liquids in porous media [13, 14, 20, 6, 8]. A commonly used modeling approach is the *crust-core* model, in which there are two regions: a dry *crust* where the water has evaporated and a wet *core*. In the crust-core approach, mass and energy equations are used to describe the heat and flow in each region, and a moving boundary tracks the evaporation front at the crust-core interface. One major concern in the deep-fat frying literature is oil uptake into the snack, and several experiments have been gathered regarding this issue [15, 21, 16, 5, 10]. However, most of these models focus on the oil absorbtion postfrying, since this is when most of the oil (approximately 80%) enters the snack [14, 20]. Another important objective of many of these studies is to predict quality changes (puffiness, shrinkage, etc.) in the snacks as they fry [10, 13, 20]. Some models also account for the decrease in the temperature of the oil due to moisture loss from the chip [13, 6].

A dominant feature of the frying process is the evaporation of the water, which can be observed both from bubbles rising to the surface and in a vapor layer surrounding the snack. Despite the formation of a vapor blanket being mentioned in several papers (see, for instance, [8] where it is stated that the bubbles impede oil inflow through the bottom boundary) this process has not been described in mathematical terms before within the deep-fat frying literature. In other contexts, film boiling has been studied and expressions for the vapor layer thickness have been derived, as well as bubble generation and release frequencies [7, 4]. However, none of the above studies address the density changes undergone due to the formation of the vapor blanket, and lift-off is not investigated at all. Furthermore, the effect of the vapor layer, which is a poor conductor, on the heat transfer in the snack is also not discussed.

In this study, we focus on predicting when a snack becomes buoyant, which happens within a few seconds of being introduced into the fryer. Thus, we do not consider structural changes, which occur later on in the frying process, nor do we consider oil-uptake, which primarily occurs postfrying. We follow the crust-core modeling approach, and we introduce the novel detail of the formation of a vapor layer under the snack. We show that the timescales associated with evaporation indicate that the formation of the vapor blanket is the dominant mechanism for lift-off. We model the growth of the vapor blanket by coupling a thin film equation to the moving-boundary problem in the snack. We show that the insulating features of the vapor blanket play an important role in the dynamics of the evaporation fronts. Whilst all of the models in the above literature are solved numerically by either finite differences or finite volumes, here we combine both numerical and analytical results and compare them together. In particular, we derive closed form solutions for the long-time behavior of the evaporation fronts and the shape of the vapor blanket, which are useful for the manufacturing process. Furthermore, we show that lift-off times are crucially dependent on the heat transfer properties of the snack.

The remainder of this paper is organized as follows. In section 2 we introduce the nondimensional mathematical model for the thermal and flow problems within the snack and vapor blanket. By exploiting the small size of some dimensionless groups, the problem simplifies to solving an energy conservation equation for each region and

Copyright © by SIAM. Unauthorized reproduction of this article is prohibited.

Downloaded 05/01/21 to 131.111.184.3. Redistribution subject to SIAM license or copyright; see https://epubs.siam.org/page/terms

a thin-film equation for the vapor blanket. A formula that relates the density of the snack to the vapor blanket thickness and the position of the evaporation fronts is also given. We first solve our model numerically in section 3 using the enthalpy method, and we are able to identify several regimes in the frying process: a heating period, the formation of the vapor blanket, and a regime where the blanket volume is constant. Motivated by these numerical results, and considering that the Stefan number of the problem is large, in section 4 we investigate a further simplification to the model, called the quasi-steady limit. In this limit, where the only time-dependence of the system originates from the motion of the evaporation fronts, we obtain analytical solutions that agree well with the numerical results and provide insight to the frying behavior. We discuss our key findings and their relevance to the snack frying process in section 5.

2. A multiphase model for snack frying. In Figure 1, we illustrate the scenario considered. We focus on the two-dimensional case, as shown in the diagram, but we keep the formulation of our mathematical model in three dimensions to be as general as possible. We propose that the snack is divided into four regions, containing different combinations of dough, water, and water vapor. Initially, we assume the dough to be entirely composed of a liquid (water) and solid phase (potato), which is defined as region 2 in our diagram. When the snack is introduced into the fryer, the water heats up and begins to evaporate, starting from the exterior. This creates two outer layers containing water vapor and solid, which we denote regions 1 and 3. As the water evaporates from the upper evaporation front, it is bubbled away into the surrounding oil. By contrast, water evaporating from the lower front forms a vapor layer beneath the snack, which we denote region 4.

In this section, we present a nondimensional mathematical model for the frying of a long thin snack, which consists of energy, mass, and momentum conservation equations for each of the different regions of the snack. We simplify these equations by exploiting small parameters in the system. For predicting lift-off time, we introduce a relation between the density of the snack, the size of the vapor blanket, and the position of the evaporation fronts.

2.1. Mathematical model. First, we present the governing equations for each of the regions in Figure 1. We keep all the equations in nondimensional form for convenience, but later we provide further discussion on the derivation, including a list of how each nondimensional parameter is defined. As illustrated in the diagram,

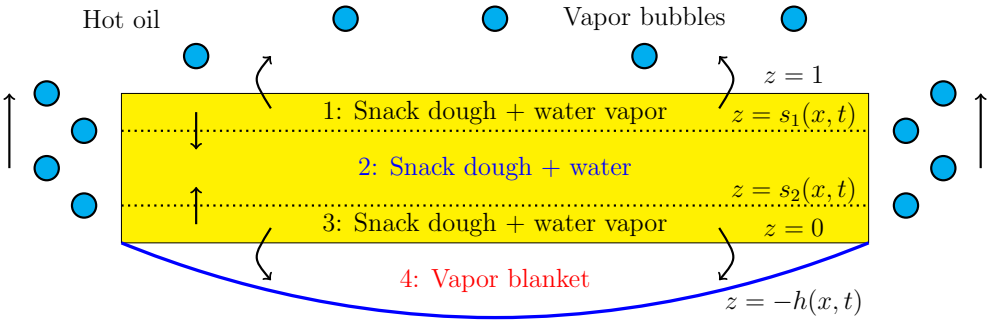

FIG. 1. *Schematic diagram of the different regions in the snack.*

Copyright © by SIAM. Unauthorized reproduction of this article is prohibited.

Downloaded 05/01/21 to 131.111.184.3. Redistribution subject to SIAM license or copyright; see https://epubs.siam.org/page/terms

the domain is long and thin with aspect ratio $\varepsilon = H/L \ll 1$ (where H and L are the height and length of the snack). We model regions 1 and 3 using an advection-diffusion equation for the temperature (due to energy conservation), and Darcy's law for the fluid flow,

$$\frac{1}{\mathrm{St}}\frac{\partial T_i}{\partial t} + \mathrm{Pe}\left(w_i\frac{\partial T_i}{\partial z} + \varepsilon^2\mathbf{u}_i\cdot\nabla_{xy}T_i\right) = \frac{\partial^2 T_i}{\partial z^2} + \varepsilon^2\nabla_{xy}^2 T_i, \qquad i = 1,3, \tag{2.1}$$

$$\mathbf{u}_i = -\nabla P_i, \qquad i = 1,3, \tag{2.2}$$

$$0 = \frac{\partial^2 P_i}{\partial z^2} + \varepsilon^2\nabla_{xy}^2 P_i, \qquad i = 1,3, \tag{2.3}$$

where $T_i(\mathbf{x}_i, t)$ is the temperature, $\mathbf{u}_i(\mathbf{x}, t) = (u_i, v_i, w_i)$ is the velocity of the fluid, and $P_i(\mathbf{x}, t)$ is the pressure. Subscripts are used to denote the different regions and $\nabla_{xy} = (\frac{\partial}{\partial x}, \frac{\partial}{\partial y}, 0)$ is the gradient in the x-y plane. Our dimensionless parameters are the Péclet number Pe, and the Stefan number St, and their definitions can be found in Table 1. We assume that the flow in the core region 2 of the snack is negligible, and so there is no need for any mass or momentum equations. The heat equation in this region is

$$\frac{\mathrm{C}}{\mathrm{St}}\frac{\partial T_2}{\partial t} = \mathrm{K}_2\left(\frac{\partial^2 T_2}{\partial z^2} + \varepsilon^2\nabla_{xy}^2 T_2\right), \tag{2.4}$$

where K_2 and C are the ratios of thermal conductivities and volumetric heat capacities between regions 2 and 1. In region 4, we have an advection-diffusion equation for the temperature and the Navier–Stokes equations for the fluid flow,

$$\frac{\mathrm{Pe}}{\mathrm{K}_4}\left(\frac{1}{\tau}\frac{\partial T_4}{\partial t} + \mathbf{u}_4\cdot\nabla T_4\right) = \frac{\partial^2 T_4}{\partial z^2} + \varepsilon^2\nabla_{xy}^2 T_4, \tag{2.5}$$

$$\mathrm{Re}\left(\frac{1}{\tau}\frac{\partial \mathbf{u}_4}{\partial t} + \mathbf{u}_4\cdot\nabla\mathbf{u}_4\right) = -\beta\left[\frac{\partial P_4}{\partial x}, \frac{\partial P_4}{\partial y}, \frac{1}{\varepsilon^2}\frac{\partial P_4}{\partial z}\right]^{\mathrm{T}} + \frac{\partial^2 \mathbf{u}_4}{\partial z^2} + \varepsilon^2\nabla_{xy}^2\mathbf{u}_4 - \frac{\mathrm{Re}}{\mathrm{Fr}^2}\hat{\mathbf{z}}, \tag{2.6}$$

$$\nabla\cdot\mathbf{u}_4 = 0, \tag{2.7}$$

where K_4 is a ratio of thermal conductivities between regions 4 and 1, τ is the ratio of the timescale of evaporation to the timescale of evolution of the vapor blanket $z = -h$, Re is the Reynolds number, Fr is the Froude number, and β is a measure of the relative size of the hydrostatic pressure of the oil acting on the gas in region 4 compared to the pressure drop needed to maintain the Darcy gas flux in regions 1 and 3. On the boundaries at $z = 1$ and $z = -h$, we have Newton's law of heating,

$$\frac{1}{\mathrm{N}}\frac{\partial T_1}{\partial z} = 1 - T_1, \qquad z = 1, \tag{2.8}$$

$$\frac{\mathrm{K}_4}{\mathrm{N}\sqrt{1+\varepsilon^2|\nabla_{xy}h|^2}}\left(\frac{\partial T_4}{\partial z} + \varepsilon^2\nabla_{xy}h\cdot\nabla_{xy}T_4\right) = T_4 - 1, \qquad z = -h, \tag{2.9}$$

where N is the Nusselt number, measuring the ratio between heat transfer at the boundary and heat conduction in the snack. At the boundary, $z = -h$, we have the kinematic and dynamic boundary conditions

Copyright © by SIAM. Unauthorized reproduction of this article is prohibited.

$$\frac{1}{\tau}\frac{\partial h}{\partial t} = w_4 - \mathbf{u}_4 \cdot \nabla_{xy} h, \qquad z = -h, \tag{2.10}$$

$$\mathbf{D} \cdot \mathbf{n} = \frac{\beta}{\varepsilon}\left(P_4 - h - \frac{\kappa}{\mathrm{Bo}}\right)\mathbf{n}, \qquad z = -h, \tag{2.11}$$

where Bo is the Bond number, κ is the curvature, D is the strain rate tensor, and $\mathbf{n}$ is the normal to the vapor blanket, given by

$$\kappa = \frac{\nabla_{xy}^2 h}{(1+\varepsilon^2|\nabla_{xy} h|^2)^{3/2}}, \tag{2.12}$$

$$\mathbf{D} = \begin{pmatrix} 2\varepsilon\frac{\partial u_4}{\partial x} & \varepsilon^2\left(\frac{\partial v_4}{\partial x} + \frac{\partial u_4}{\partial y}\right) & \varepsilon^2\frac{\partial w_4}{\partial x} + \frac{\partial u_4}{\partial z} \\ \varepsilon^2\left(\frac{\partial u_4}{\partial y} + \frac{\partial v_4}{\partial x}\right) & 2\varepsilon\frac{\partial v_4}{\partial y} & \varepsilon^2\frac{\partial w_4}{\partial y} + \frac{\partial v_4}{\partial z} \\ \frac{\partial u_4}{\partial z} + \varepsilon^2\frac{\partial w_4}{\partial x} & \frac{\partial v_4}{\partial z} + \varepsilon^2\frac{\partial w_4}{\partial y} & 2\varepsilon\frac{\partial w_4}{\partial z} \end{pmatrix}, \tag{2.13}$$

$$\mathbf{n} = \frac{1}{\sqrt{1+\varepsilon^2|\nabla_{xy} h|^2}}\begin{pmatrix} -\varepsilon\frac{\partial h}{\partial x} \\ -\varepsilon\frac{\partial h}{\partial y} \\ 1 \end{pmatrix}. \tag{2.14}$$

On the evaporation fronts, $z = s_i$ for $i = 1, 2$, we require that the temperature matches the evaporation temperature of water

$$T_1 = T_2 = 0, \qquad z = s_1, \tag{2.15}$$

$$T_2 = T_3 = 0, \qquad z = s_2. \tag{2.16}$$

We also have a Stefan condition describing the motion of the evaporation fronts. This condition can be derived by balancing the latent energy required to vaporize water with difference in heat flux on either side of the boundary. This gives us

$$\dot{s}_1 = \mathrm{K}_2\frac{\partial T_2}{\partial z} - \frac{\partial T_1}{\partial z} + \varepsilon^2\nabla_{xy} s_1 \cdot \nabla_{xy}(T_1 - \mathrm{K}_2 T_2), \qquad z = s_1, \tag{2.17}$$

$$\dot{s}_2 = \mathrm{K}_2\frac{\partial T_2}{\partial z} - \frac{\partial T_3}{\partial z} + \varepsilon^2\nabla_{xy} s_2 \cdot \nabla_{xy}(T_3 - \mathrm{K}_2 T_2), \qquad z = s_2. \tag{2.18}$$

The change in density undergone when the water vaporizes creates a flow in regions 1 and 3. As discussed by [17], the equations that describe the flow generated by this volume change are

$$\left(1 - \frac{1}{\mathrm{R}}\right)\dot{s}_1 = -w_1 + \varepsilon^2\mathbf{u}_1 \cdot \nabla_{xy} s_1, \qquad z = s_1, \tag{2.19}$$

$$\left(1 - \frac{1}{\mathrm{R}}\right)\dot{s}_2 = -w_3 + \varepsilon^2\mathbf{u}_3 \cdot \nabla_{xy} s_2, \qquad z = s_2, \tag{2.20}$$

where R is the ratio of the density of water to the density of steam. This signifies the volume change that happens when the water is vaporized, which drives the gas flow.

Finally, at the interface between the snack and the vapor blanket, we have continuity of temperature, mass, pressure, and heat flux,

$$T_3 = T_4, \quad P_3 = \varepsilon^{-2}\beta\Gamma P_4, \quad \mathrm{K}_4\frac{\partial T_4}{\partial z} = \frac{\partial T_3}{\partial z}, \qquad z = 0, \tag{2.21}$$

$$\left[\varepsilon^2 u_3, \varepsilon^2 v_3, w_3\right] = \left[u_4, v_4, w_4\right], \qquad z = 0, \tag{2.22}$$

Copyright © by SIAM. Unauthorized reproduction of this article is prohibited.

Downloaded 05/01/21 to 131.111.184.3. Redistribution subject to SIAM license or copyright; see https://epubs.siam.org/page/terms

Downloaded 05/01/21 to 131.111.184.3. Redistribution subject to SIAM license or copyright; see https://epubs.siam.org/page/terms

where Γ is the nondimensional permeability of the snack. The dimensionless initial conditions are given by

$$T_2(\mathbf{x}, t) = T^*, \tag{2.23}$$

$$s_1(x, y, 0) = 1, \tag{2.24}$$

$$s_2(x, y, 0) = 0, \tag{2.25}$$

$$h(x, y, 0) = 0. \tag{2.26}$$

In Table 1 we list the dimensionless parameters of the system, their definitions in terms of dimensional parameters, and their approximate values. The dimensional parameters appearing in Table 1 are L_v, the latent heat of vaporization of water; ϕ, the porosity of the snack; χ, the permeability of the snack; h_c, the heat transfer coefficient; γ, the interfacial tension between water and oil; g, the acceleration due to gravity; H, the height of the snack; L, the length of the snack; μ_v, the viscosity of water vapor; T_o, T_l, T_a, the temperature of the oil, the evaporation temperature of water, and the ambient air temperature of the snack before entry into the oil; and ρ_o, ρ_l, ρ_v, the density of oil, water, and vapor, respectively. Finally, we have some compound parameters for regions 1, 2, and 3, each with a subscript denoting the relevant region. These are ρ_j, the compound density; k_j the compound thermal conductivity; and $c_{p,j}$, the compound specific heat capacity, with $j = 1 - 4$. These compound parameters have been determined by taking a volume-weighted average of the parameters for the individual phases (solid snack, water, vapor) in each region (see [11], for instance). For example, $\rho_1 = \alpha_s \rho_s + \alpha_v \rho_v$, where each α represents a mass fraction.

2.2. Model simplifications. Having calculated the nondimensional parameters in Table 1, we are motivated to consider the asymptotic limit of

$$\mathrm{Pe},\ \varepsilon,\ \mathrm{Re},\ \mathrm{Bo}^{-1},\ \mathrm{Pe/K_4},\ \mathrm{Pe/K_4}\tau,\ \mathrm{Re}/\tau,\ \varepsilon^2\mathrm{K_2},\ \mathrm{Re/Fr}^2,\ 1/\mathrm{R} \to 0. \tag{2.27}$$

Note that although a few of these parameter groups associated with the vapor layer (Re, $\mathrm{Pe/K_2}$) are marginal in this scaling, we have also carried out a more complex scaling in which the thicknesses of regions 3 and 4 are scaled separately. This scaling confirms that all the dimensionless quantities listed above are small.

TABLE 1
Dimensionless parameters and their approximate numerical values.

Parameter	Definition	Value
St	$L_v\phi\rho_l/(\rho_1 c_{p,1}(T_o - T_e))$	8.4
C	$c_{p,2}\rho_2/(c_{p,1}\rho_1)$	2.1
ε	H/L	1.1×10^{-2}
Pe	$c_{p,4}(T_o - T_e)/L_v$	5.8×10^{-2}
$\mathrm{K_2}$	k_2/k_1	1.4
$\mathrm{K_4}$	k_4/k_1	4.2×10^{-2}
τ	$\phi\rho_l/\rho_v$	5.8×10^{2}
Re	$k_1(T_o - T_e)/(L_v\mu_v)$	9.2×10^{-1}
β	$L_v g\rho_v\rho_o H^5/(k_1 L^2\mu_v(T_o - T_e))$	6.5×10^{-1}
Γ	χ/H^2	2.0×10^{-4}
N	$h_c H/k_1$	1.3
T^*	$(T_\mathrm{a} - T_e)/(T_o - T_e)$	-1.1
Bo	$\rho_o g L^2/\gamma$	1.1×10^{3}
R	ρ_l/ρ_v	1.7×10^{3}
Fr	$(k_1(T_o - T_e)/\rho_v L_v H^2)\sqrt{L/g}$	4.3

Copyright © by SIAM. Unauthorized reproduction of this article is prohibited.

Downloaded 05/01/21 to 131.111.184.3. Redistribution subject to SIAM license or copyright; see https://epubs.siam.org/page/terms

Under these limits, the only coupling between the flow and thermal problems is through the boundary conditions (2.10), (2.11), (2.19), and (2.20). The simplified governing equations for the heat problem are

$$\frac{1}{\mathrm{St}}\frac{\partial T_1}{\partial t} = \frac{\partial^2 T_1}{\partial z^2}, \qquad s_1 \le z \le 1, \tag{2.28}$$

$$\frac{\mathrm{C}}{\mathrm{St}}\frac{\partial T_2}{\partial t} = \mathrm{K}_2\frac{\partial^2 T_2}{\partial z^2}, \qquad s_2 \le z \le s_1, \tag{2.29}$$

$$\frac{1}{\mathrm{St}}\frac{\partial T_3}{\partial t} = \frac{\partial^2 T_3}{\partial z^2}, \qquad 0 \le z \le s_2. \tag{2.30}$$

The only dependence of the heat problem on the thickness of the vapor blanket h is through the lower boundary condition. Hence, the complete set of boundary conditions for the heat problem are

$$\frac{1}{\mathrm{N}}\frac{\partial T_1}{\partial z} = 1 - T_1, \qquad z = 1, \tag{2.31}$$

$$T_1 = T_2 = 0, \qquad z = s_1, \tag{2.32}$$

$$\dot{s}_1 = \mathrm{K}_2\frac{\partial T_2}{\partial z} - \frac{\partial T_1}{\partial z}, \qquad z = s_1, \tag{2.33}$$

$$T_2 = T_3 = 0, \qquad z = s_2, \tag{2.34}$$

$$\dot{s}_2 = \mathrm{K}_2\frac{\partial T_2}{\partial z} - \frac{\partial T_3}{\partial z}, \qquad z = s_2, \tag{2.35}$$

$$\frac{1}{\mathrm{N}}\frac{\partial T_3}{\partial z}\left(\frac{h\mathrm{N}}{\mathrm{K}_4} + 1\right) = T_3 - 1, \qquad z = 0, \tag{2.36}$$

where (2.36) is derived by solving for T_4 and inserting the solution into (2.21). Specifically, T_4 is given in terms of T_3 and h by

$$T_4 = 1 + \frac{1}{\mathrm{N}}\left(\frac{(z+h)\mathrm{N}}{\mathrm{K}_4} + 1\right)\left.\frac{\partial T_3}{\partial z}\right|_{z=0}. \tag{2.37}$$

In order to obtain an equation for h, we need to follow a series of steps. Firstly, taking the third component of the simplified version of (2.6) together with the reduced form of (2.11) we obtain $P_4 = h$ throughout region 4. Now, $\mathbf{u}_4$ can be found simply by integrating the reduced form of the first two components of (2.6), as well as (2.7). Substituting this into the kinematic condition (2.10) gives

$$\frac{1}{\tau}\frac{\partial h}{\partial t} = \frac{\beta}{3}\nabla_{xy}\cdot\left(h^3\nabla_{xy}h\right) - w_4|_{z=0}. \tag{2.38}$$

Finally, by considering the fluid problem in region 3, and using the simplified version of (2.20), we see that $w_4|_{z=0} = -\dot{s}_2$. Thus, the governing thin-film equation for the vapor blanket becomes

$$\frac{1}{\tau}\frac{\partial h}{\partial t} = \frac{\beta}{3}\nabla_{xy}\cdot\left(h^3\nabla_{xy}h\right) + \dot{s}_2. \tag{2.39}$$

We would expect that at the edges of the snack, h would take some finite value and the pressure would be equivalent to the hydrostatic pressure of the oil. However, in our thin film equation (2.39) we cannot impose both these conditions, so we choose

$$h = 0, \text{ at } \delta\Omega_0 \tag{2.40}$$

Copyright © by SIAM. Unauthorized reproduction of this article is prohibited.

as the lateral boundary condition, where Ω_0 is the cross-section of the snack at $z = 0$, and $\delta\Omega_0$ is the boundary of Ω_0. We note that in choosing this boundary condition, we will see that the h will have to have infinite slope at the edges in order to have a finite flux.

Note that whilst the vapor blanket thickness depends spatially on x and y, $h = h(x, y, t)$, the temperature only depends on z, except for the boundary condition (2.36). Hence, it is convenient to replace h in (2.36) by an average film thickness $\overline{h} = \int_{\partial\Omega_0} h\, dxdy$. Making this substitution, the thermal problem is purely in terms of z, and the vapor blanket problem is in terms of x and y. We can simplify even further by assuming that the snack is uniform in the y direction, giving us a one-dimensional model for the thermal problem in z and a one-dimensional model for the vapor blanket problem in x. This is the approach taken for the remainder of this study.

2.3. Density calculation and lift-off time. A necessary condition for the snack to detach from the conveyor belt is that its density is less than that of the surrounding oil. The reduction of the density of the snack is due to two processes. Firstly there is loss of mass as water evaporates into steam and leaves the snack. Secondly the formation of the vapor blanket increases the volume of the snack.

The dimensionless density, ρ, is scaled by the density of oil, ρ_o, so that $\rho = 1$ when the snack is neutrally buoyant. The density is given by

(2.41)

$$\rho(t) = \frac{1}{1 + \int_0^1 h\,\mathrm{d}x}\left(\frac{\rho_v}{\rho_o}\int_0^1 h\,\mathrm{d}x + \frac{\rho_l}{\rho_o}\alpha_l(s_1 - s_2) + \frac{\rho_v}{\rho_o}\alpha_v\left[1 - (s_1 - s_2)\right] + \frac{\rho_s}{\rho_o}\alpha_s\right).$$

The denominator is the volume of the snack, including the volume of the bubble given by integrating over h. The numerator is the mass of the snack broken into contributions from the gas in the bubble, liquid water in region 2, water vapor in regions 1 and 3, and the solid component of the snack. Therefore, the nondimensional lift-off time, which we denote t^*, is the first time[1] for which

$$\rho(t^*) < 1. \tag{2.42}$$

3. Numerical approach. Our first approach is to solve (2.28)–(2.30), (2.39) numerically using the enthalpy method [3, 18]. The nondimensional temperature, T, is related to the nondimensional enthalpy, θ, in the following way:

$$T = \begin{cases} \frac{\mathrm{StK}_2}{C}\theta : & \theta < 0, \\ 0 : & 0 \le \theta \le 1, \\ \mathrm{St}(\theta - 1) : & \theta > 1. \end{cases} \tag{3.1}$$

The enthalpy method conveniently reduces the problem to solving the single partial differential equation

$$\frac{\partial\theta}{\partial t} = \frac{\partial^2 T}{\partial z^2} \tag{3.2}$$

[1]Note that in reality, there may be some surface tension effects holding the snack down to the solid substrate, therefore delaying lift-off time. However, since these depend on the specific surface properties of the fryer substrate, we do not study such effects here.

Copyright © by SIAM. Unauthorized reproduction of this article is prohibited.

Downloaded 05/01/21 to 131.111.184.3. Redistribution subject to SIAM license or copyright; see https://epubs.siam.org/page/terms

within the entire domain $0 \leq z \leq 1$, where θ and T are related via (3.1). We solve (2.39) and (3.2) using the method of lines with a fourth order central finite difference scheme in space and a fourth order explicit Runge–Kutta scheme in time, where at each time step we update T using the relation (3.1). It is possible to achieve even greater accuracy using other more detailed schemes, such as adaptive time-stepping and spectral methods, but we find that our current approach is well within the convergence regime and is sufficiently accurate for the purposes of this study.

We plot the solution in Figures 2 and 3, illustrating the evolution of the temperature, the vapor blanket, and the resultant snack density. We identify several clear regimes in the frying process, which we indicate in the density plot in Figure 3a. Initially the snack is plunged into the oil at room temperature, and so the first regime consists of a heating period, bringing the temperature within the snack to the evaporation temperature. During this *heat diffusion* regime, the snack is entirely

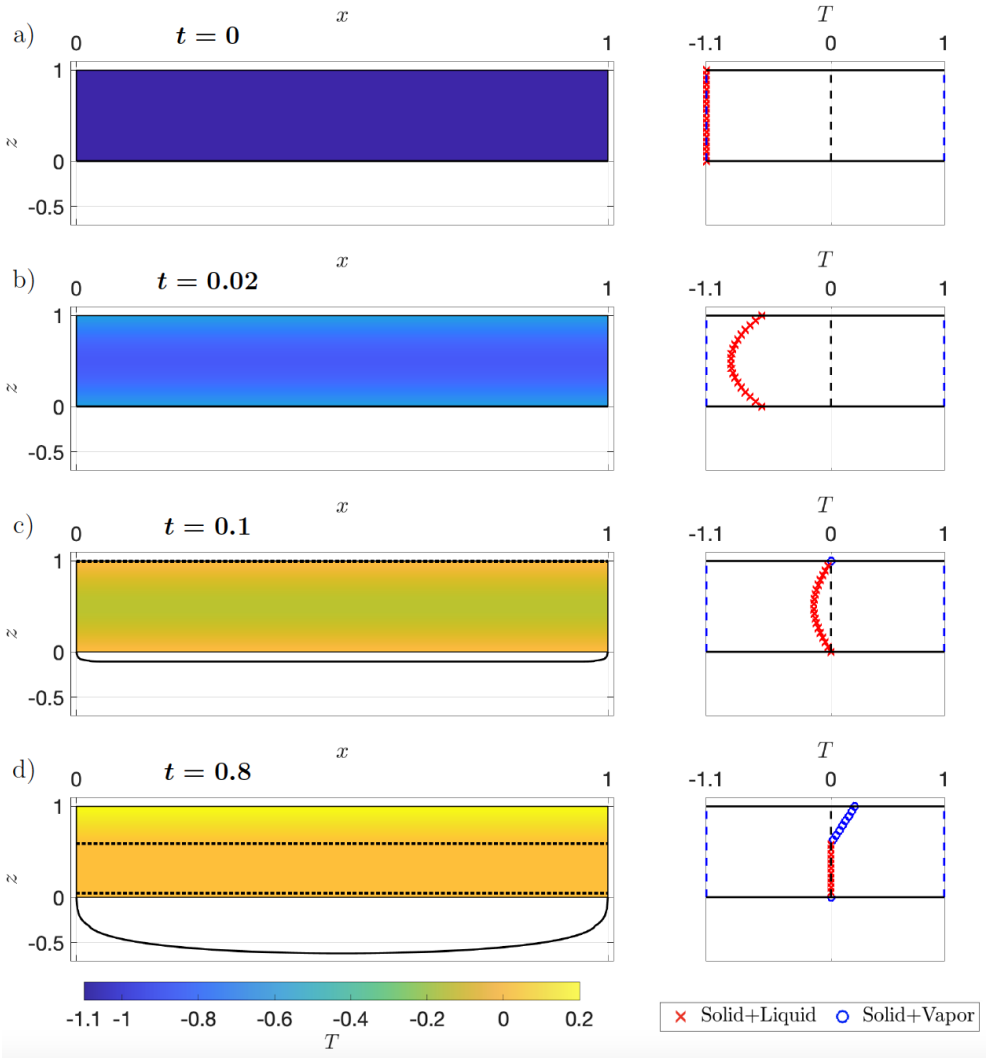

FIG. 2. (a,b,c,d) *Numerical solution at* $t = 0, 0.02, 0.1, 0.8$*, showing a color plot of the temperature in the snack, a corresponding line plot of the temperature, and the film thickness beneath the snack.*

Copyright © by SIAM. Unauthorized reproduction of this article is prohibited.

Downloaded 05/01/21 to 131.111.184.3. Redistribution subject to SIAM license or copyright; see https://epubs.siam.org/page/terms

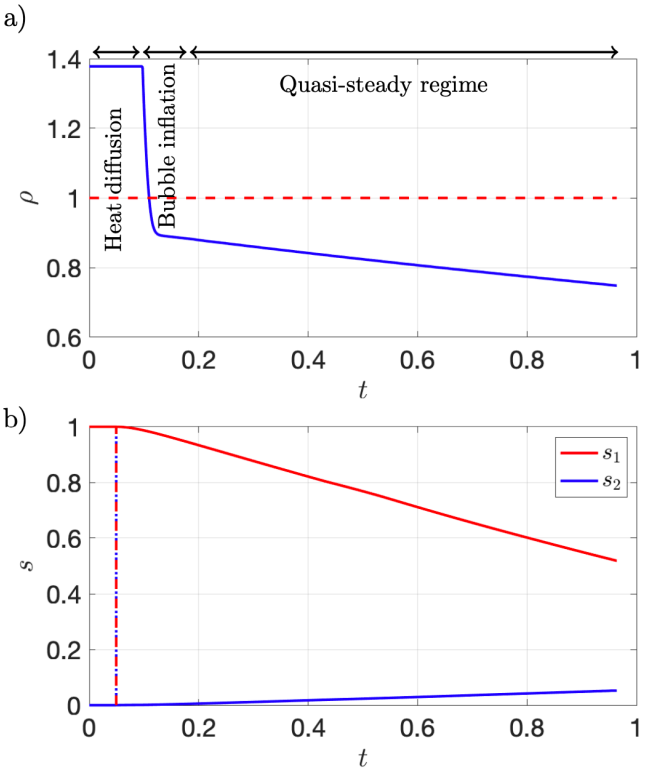

FIG. 3. (a) *Numerical solution for the density evolution over time, indicating the critical density for lift-off* $\rho = 1$. (b) *Evolution of the evaporation fronts* s_1 *and* s_2.

composed of liquid and solid (region 2). Once the temperature is near the boiling point everywhere and equal to the boiling temperature at the edges of the snack, the latent heat begins to be removed. As the latent heat is removed from the edges of the snack, two evaporation fronts recede into the interior of the snack, bubbling away vapor through the top and bottom. This is the second regime of the process, during which the vapor blanket is formed and inflates very rapidly, causing a sudden drop in density. Hence, this is denoted the *bubble inflation* regime. However, the vapor blanket quickly reaches a steady state, bringing us to the third and final regime of the process. During this regime, even though the blanket thickness is approximately constant, the evaporation fronts continue to move inwards, and so we denote this the *quasi-steady regime*. In particular, the fact that the blanket remains at near-constant volume can only be explained by a constant growth rate of the evaporation front $\dot{s}_2$ in (2.39), and this is in accordance with our numerical observations in Figure 3b. Furthermore, the temperature within each region is approximately linear with z, as can be seen in Figure 2d. This piecewise linear temperature profile, which is characteristic of the quasi-steady limit [3, 12, 2], is due to the large Stefan number in (2.28)–(2.30). Later in section 4 we will use our numerical observations from Figure 2d to motivate an asymptotic treatment of the quasi-steady behavior by taking the limit of large Stefan number. We also note that, as mentioned at the end of section 2.2, the slope of the blanket at the edges of the snack is infinite, which is most visible in Figure 2d. Thus, we have used a refined spatial grid in the numerical solution.

Copyright © by SIAM. Unauthorized reproduction of this article is prohibited.

Downloaded 05/01/21 to 131.111.184.3. Redistribution subject to SIAM license or copyright; see https://epubs.siam.org/page/terms

Downloaded 05/01/21 to 131.111.184.3. Redistribution subject to SIAM license or copyright; see https://epubs.siam.org/page/terms

The lift-off time of the snack is taken as the time at which the density falls below the oil density (2.42). For the parameters used here, this corresponds to a time of $t \approx 0.1$, or in dimensional terms, ~ 1 second, which is in agreement with observations in the frying industry. A key result from our model is that the lift-off time is largely controlled by the inflation of the vapor blanket. In fact, since the bubble inflation is so rapid and causes such a large relative change in volume, the time for lift-off is only marginally larger than the time needed for first evaporation (see Figure 3a). Hence, as a proxy for the lift-off time, one can simply solve the initial heat diffusion problem (first regime) and find the time at which the latent heat is first removed from the bottom boundary $z = 0$. Such an approach reduces the computational cost and technical complexity of the problem since it avoids having to resolve the growth of the vapor blanket. Following this proxy approach, the key parameter that determines the lift-off time is the Nusselt number N, which is a measure of the ratio between heat transfer at the boundary and heat conduction in the snack. We can further simplify this proxy problem in order to derive an analytic formula for t^* as a function of N. We do this by integrating the heat equation from the bottom to the top of the crisp, substituting in the Newton heating boundary conditions, then assuming the average temperature in the crisp and the temperature at the top and bottom of the crisp are all approximately equal. Doing this we recover an ODE for the temperature of the crisp, which we can solve to recover

$$t^*(N) = \frac{C}{2\mathrm{NStK}_2} \log\left(1 - T^*\right). \tag{3.3}$$

In the literature the Nusselt number for snacks varies between 0.3 and 1.3. Therefore, in Figure 4 we plot the variation of approximate lift-off time with Nusselt number calculated using the analytic formula, the proxy approach, and the full numerical problem for t^* such that $\rho(t^*) < 1$. The lift-off time is a monotone decreasing function of N, as expected. In dimensional terms lift-off occurs for times between 0.5 and 2.6 seconds.

As a further motivation for our vapor blanket model, suppose instead we were to ignore the vapor blanket and just solve the classic Stefan problem with Newton

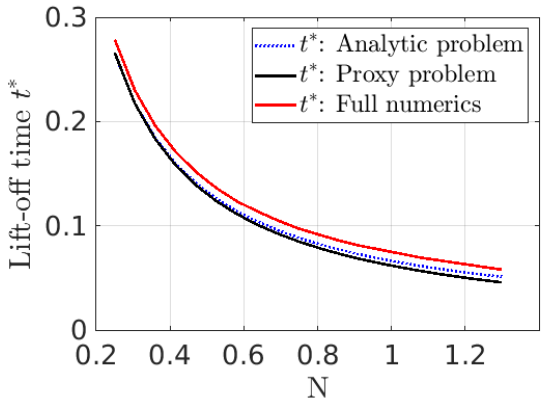

FIG. 4. *Variation of the nondimensional lift-off time with Nusselt number* N*, showing the analytic times, the approximate times calculated by solving the proxy heat diffusion problem until first evaporation, and the precise times calculated by solving the full numerical problem until* $\rho(t^*) < 1$.

Copyright © by SIAM. Unauthorized reproduction of this article is prohibited.

Downloaded 05/01/21 to 131.111.184.3. Redistribution subject to SIAM license or copyright; see https://epubs.siam.org/page/terms

heating boundary conditions (i.e., $h = 0$). In this case, we skip the second regime since there is no bubble inflation and simply move from a heat diffusion regime to a quasi-steady regime. From Figure 3a we see that the density decay in the quasi-steady regime is much slower than that caused by bubble inflation. This results in a lift-off time closer to $t = 1$, which in dimensional terms corresponds to more than 10 seconds, and this is a factor of ten larger than experimental observations. Hence, this serves as a good indication that our vapor blanket model is accurate and provides the essential ingredients to predict the lift-off time during frying.

Motivated by the above simulations, we now consider a further limiting case of the mathematical model called the quasi-steady limit. In this limit, we can further simplify the governing equations and find some analytical results that provide useful insight to the problem.

4. Quasi-steady limit. The quasi-steady limit corresponds to when the thermal problem (2.28)–(2.30) becomes independent of time except through the motion of the evaporation fronts. This limit, which is typical in such phase change problems, is a result of the fact that the Stefan number is large [3, 12, 2]. In our case, $\mathrm{St} = O(10)$, which, though not large in the absolute sense, is large enough for the purposes of our asymptotic analysis, as the numerical results suggest. It is often the case that an asymptotic result valid when a certain parameter is large is also valid beyond this range. To study this limit, we restrict our attention to the second and third regimes of the above simulations. That is to say, we replace the initial conditions at room temperature (2.23) that we used previously with initial conditions at the evaporation temperature $T(t = 0) = 0$. As before, we restrict our attention to the case where the evaporation fronts move uniformly, such that s_1, s_2, and T_1–T_3 are independent of x and y. Hence, the temperature in each region is given by

$$T_i = A_i(t)z + B_i(t) \tag{4.1}$$

for some functions A_i, B_i, for $i = 1 - 4$. The thermal profiles (4.1) are consistent with our numerical observations in Figure 2d, where the temperature is approximately linear within each region.

Applying the boundary conditions (2.31)–(2.36), we obtain

$$T_1 = \frac{z - s_1}{1 + 1/\mathrm{N} - s_1}, \tag{4.2}$$

$$T_2 = 0, \tag{4.3}$$

$$T_3 = \frac{s_2 - z}{1/\mathrm{N} + \overline{h}/\mathrm{K}_4 + s_2}, \tag{4.4}$$

$$\dot{s}_1 = \frac{-1}{1 + 1/\mathrm{N} - s_1}, \tag{4.5}$$

$$\dot{s}_2 = \frac{1}{1/\mathrm{N} + \overline{h}/\mathrm{K}_4 + s_2}. \tag{4.6}$$

The last equation (4.6) contains the spatial average of the vapor blanket thickness, $\overline{h} = \int_0^1 h \, \mathrm{d}x$, which is found by solving the thin-film equation

$$\frac{1}{\tau}\frac{\partial h}{\partial t} = \frac{\beta}{3}\frac{\partial}{\partial x}\left(h^3 \frac{\partial h}{\partial x}\right) + \frac{1}{1/\mathrm{N} + \overline{h}/\mathrm{K}_4 + s_2}, \tag{4.7}$$

Copyright © by SIAM. Unauthorized reproduction of this article is prohibited.

Downloaded 05/01/21 to 131.111.184.3. Redistribution subject to SIAM license or copyright; see https://epubs.siam.org/page/terms

together with the boundary conditions $h = 0$ at $x = 0, 1$ from (2.40). We again note that we expect the slope of h to be infinite at the edges to be consistent with the requirement for a finite nonzero flux. We can solve (4.5) immediately, finding

$$s_1 = \frac{1}{\mathrm{N}}\left(1 + \mathrm{N} - \sqrt{1 + 2\mathrm{N}^2 t}\right). \tag{4.8}$$

The form of (4.8) reveals the classic $t^{1/2}$ similarity behavior that is discussed for Stefan problems in the literature [19, 9]. The remaining unknowns h and s_2 are found by solving the coupled system (4.6)–(4.7). In Figure 5 we display the numerical solution to this system, calculated using the method of lines, as before. We see a fast early time growth of the evaporation front s_2, causing a rapid inflation of the bubble over a timescale of around $t = 0.01$. After this inflation period, the growth rate of s_2 is almost constant, and consequently the bubble shape reaches a steady state, which is consistent with Figures 2 and 3.

To understand the apparent steady state, let us consider the evolution equation for the lower evaporation front (4.6). It is not immediately obvious that (4.6) yields a constant growth rate solution. However, the nondimensional conductivity ratio is very small $\mathrm{K}_4 \approx 0.04$, and s_2 in Figure 5 is also very small, suggesting that perhaps the variables s_2 and h ought to be rescaled by K_4 appropriately. Since, for the steady state solution, we expect h to be independent of time but dependent on space, and we expect the evaporation front to move at a linear growth rate, we seek a rescaling of the form

$$s_2 = \mathrm{K}_4^c(a + bt) + \mathcal{O}(\mathrm{K}_4^{2c}), \tag{4.9}$$

$$h = \mathrm{K}_4^d H(x) + \mathcal{O}(\mathrm{K}_4^{2d}) \tag{4.10}$$

for some unknown coefficients $a, b, c, d > 0$. By inserting the above into (4.6)–(4.7), we can see that a steady state is only possible (to leading order) if we choose

$$d - 1 + c = 0, \tag{4.11}$$

$$4d = c, \tag{4.12}$$

which has solution $c = 4/5$ and $d = 1/5$. Taking the limit of small K_4, the resulting system of equations is

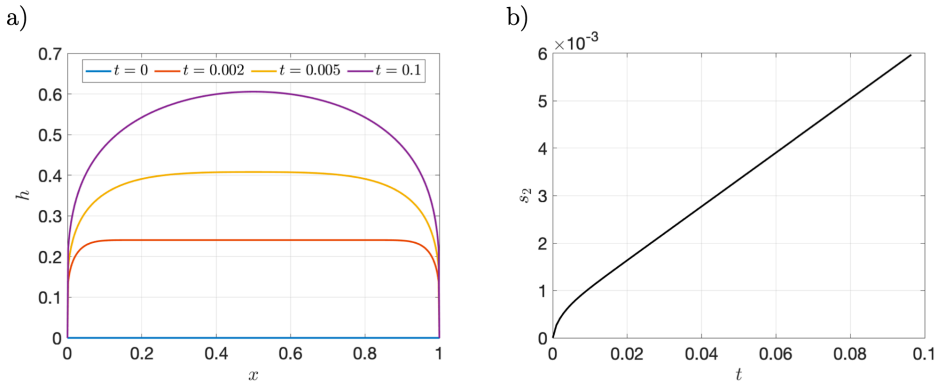

FIG. 5. *Solution to the quasi-steady approximation.* (a) *Evolution of the thin film h at various times.* (b) *Evolution of the lower evaporation front $s_2(t)$.*

Copyright © by SIAM. Unauthorized reproduction of this article is prohibited.

$$b = \frac{1}{\beta \overline{H}}, \tag{4.13}$$

$$\frac{1}{3}\left(H^3 H_x\right)_x + \frac{1}{\beta \overline{H}} = 0, \tag{4.14}$$

where $\overline{H} = \int_0^1 H \, \mathrm{d}x$ is the scaled average film thickness, which is a constant in the steady state. We can solve (4.14) to give H in terms of its average value

$$H = \left(\frac{6x(1-x)}{\overline{H}\beta}\right)^{1/4}, \tag{4.15}$$

where we notice that the slope of H is indeed infinite at $x = 0, 1$. $\overline{H}$ is found by integrating (4.15), which gives

$$\overline{H} = \left[\frac{\Gamma(5/4)}{\Gamma(3/4)}\left(\frac{8\pi^2}{27\beta}\right)^{1/4}\right]^{4/5}, \tag{4.16}$$

where Γ is the Euler Gamma function. Note that the above is only valid for times much smaller than $t \approx \mathrm{K}_4^{-4/5} \approx 13$. However, the snack frying process all takes place within $0 \leq t \leq 1$, so this is acceptable. Note also that the linear behavior of s_2 with respect to time is different from the square root behavior of s_1 observed in (4.8). Hence, the vapor blanket completely changes evaporation at the lower boundary.

In Figure 6 we display a comparison of the results from the quasi-steady limit, including the steady state, to the original numerical solution from Figures 2 and 3. For the comparison, we look at the long-time evolution of the film thickness, the density, the evaporation fronts, and the temperature within the snack. We see that in all cases there is close agreement between the numerical solution to the full problem, the quasi-steady solution, and the steady state. There is a slight discrepancy ($\sim$5%) for the steady state solution to the thin film, and this can be explained by the asymptotic approximation (4.10) and the fact that the Stefan number is not very large. Indeed, the correction to the leading-order approximation in 1/St is $O(1/\mathrm{St})$, which is comparable to the magnitude of the discrepancy we see between the numerical solution to the full problem and the quasi-steady result. This discrepancy could be mitigated by going to higher-order terms in the asymptotic expansions.

There is also a slight disagreement ($\sim$1%) between the early time density predictions of the numerical solution to the full problem and the quasi-steady solution. This can be explained by the way in which we calculate the speed of the lower evaporation front $\dot{s}_2$, which largely controls the density at early times via the inflation of the vapor blanket. In the quasi-steady approximation we calculate the evaporation front s_2 using a numerical discretization scheme in time to solve (4.6), with time step $\delta t = 4 \times 10^{-8}$, providing very smooth results. On the other hand, in the numerical solution to the full problem, since we calculate the temperature using the enthalpy method, which does not require tracking the position of the fronts, the evaporation front is calculated by finding the grid point that separates liquid and gas phases. Since the grid spacing is finite, this leads to nonsmooth step changes in s_2 and spikes in the time-derivative of s_2, which we have attempted to smooth using a damping method. Nevertheless, even with a time step $\delta t = 4 \times 10^{-8}$, this produces inevitable error associated with the inflation of the vapor blanket, and this is reflected in the slight disagreement for the density prediction at early times.

Copyright © by SIAM. Unauthorized reproduction of this article is prohibited.

Downloaded 05/01/21 to 131.111.184.3. Redistribution subject to SIAM license or copyright; see https://epubs.siam.org/page/terms

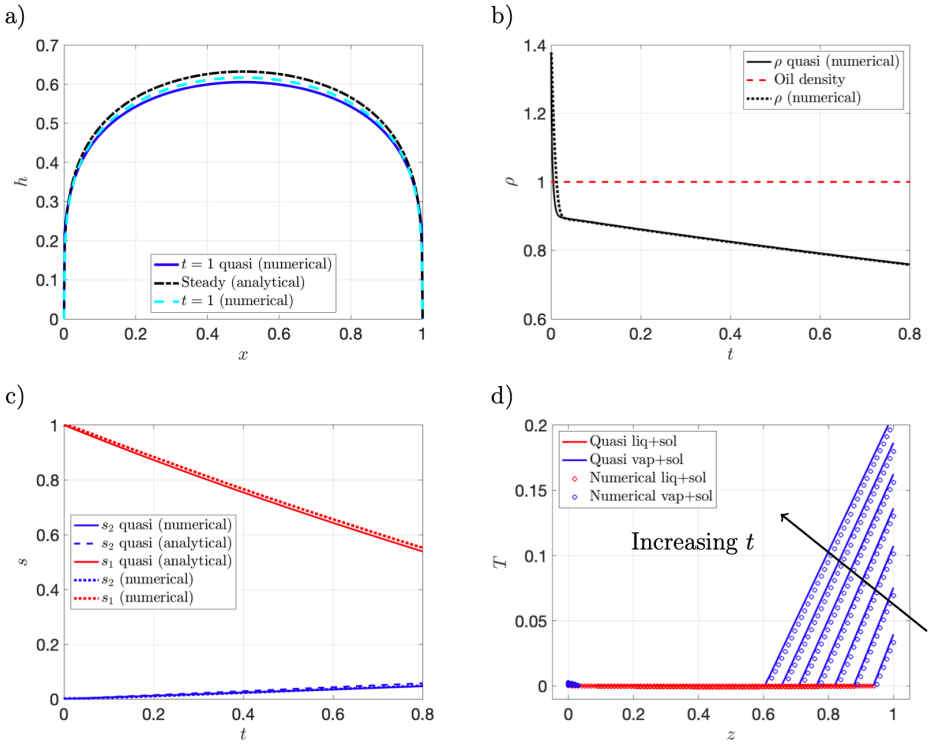

FIG. 6. *Long time results from the quasi-steady approximation.* (a) *Evolution of the thin film* h *at various times, compared to the analytical solution for the steady state.* (b) *Density* $\rho(t)$ *as a function of time, indicating the lift-off density* $\rho = 1$. (c) *Evolution of the lower Stefan boundary* $s_2(t)$*, compared to the analytical solution for the steady state* $\dot{s}_2 = K_4^{4/5}/\overline{H}$. (d) *Temperature profiles* $T(z,t)$ *at different times between* $t = 0$ *and* $t = 1$*, indicating liquid and vapour regions.*

Closer agreement can be attained with an even smaller spatial discretization, but due to the explicit discretization method, this results in lengthy computation times. Hence, interestingly the quasi-steady solution, though it only applies to an asymptotic limit, is generally more accurate than the numerical solution to the full problem. Since the critical time of interest is the lift-off time, which still shows close agreement between these two approaches, we do not consider this discrepancy to be very important.

Finally, in Figure 6 c,d we display a comparison of the predictions of the evaporation fronts and the temperature. On a macroscopic level, there is very close agreement, and in particular the steady state solution performs remarkably well. After a time of $t = 1$, or 10 seconds in dimensional terms, nearly half the liquid in the snack has evaporated and the density has dropped by a factor of around 2. The overall thickness of the vapor blanket is nearly equal to the total width of the snack, which is also consistent with experimental observations.

5. Conclusions. We considered a mathematical model of potato snack frying to estimate the time at which the snack becomes less dense than the surrounding oil and begins to float, also known as the lift-off time. To that end, we modeled the frying process as a Stefan problem with two propagating evaporation fronts at which the liquid in the dough evaporates, thereby decreasing the density of the snack. In addition,

Copyright © by SIAM. Unauthorized reproduction of this article is prohibited.

Downloaded 05/01/21 to 131.111.184.3. Redistribution subject to SIAM license or copyright; see https://epubs.siam.org/page/terms

Downloaded 05/01/21 to 131.111.184.3. Redistribution subject to SIAM license or copyright; see https://epubs.siam.org/page/terms

a key feature in our model is the presence of a vapor blanket that forms underneath the snack as liquid evaporates. The moving evaporation fronts and the vapor blanket were assumed to be the two main mechanisms for density reduction of the snack and, therefore, its eventual lift-off. Numerical results of the full system, using the enthalpy method, revealed that both of these mechanisms were indeed essential to predict a physically realistic lift-off time of the order of one second.

Two simplifications to the model were presented which gave useful insights into the frying process and reduced the computation time. Firstly, since the inflation of the vapor blanket causes a significant decrease in the snack density over a very short timescale, we demonstrated that the lift-off time could be well approximated by the time for first evaporation instead. This calculation is computationally cheaper and less technically complex since it avoids modeling the vapor blanket dynamics. Secondly, due to the large Stefan number we considered a simplified quasi-steady model to describe the late-time dynamics. Both numerical and analytical solutions to this simplified model were presented, showing close agreement with solutions to the full system. This quasi-steady approximation not only further reduces the computational cost but also provides key insights such as the steady-state shape of the vapor blanket at late times.

One of the key dimensionless parameters that emerged as part of our analysis was the Nusselt number N, which is the ratio between heat transfer at the snack boundary and heat conduction in the snack interior. We investigated how changing this parameter affects the lift-off time of the snack, which is important for snack manufacturers since changing the dough, for example, can alter the Nusselt number via the material properties. Hence, knowledge of the dependence of the lift-off time on N is useful in determining optimal cooking strategies.

To further improve the prediction of lift-off time, other forces on the snack could be considered. These could include interfacial tension between the snack and its substrate (the conveyor belt) as well as the peeling energy required to overcome the dough elasticity. As a result, the orientation of the snack on the belt and indeed the belt design and material could have a further impact on the lift-off time of the snack.

Acknowledgments. The authors would like to aknowledge the 138th European Study Group with Industry which was held in Bath, 16-20 July 2018, and jointly hosted by the University of Bath and University of Bristol. The authors are also thankful to all the participants of the ESGI project for useful discussions: Peter Baddoo (University of Cambridge, UK), Sean Bohun (University of Ontario, Canada), Stephen Cowley (University of Oxford, UK), Helen Fletcher (University of Oxford, UK), Harry Reynolds (University of Oxford, UK), and Chris Sear (University of Cambdrige, UK). Special thanks to PepsiCo for proposing the problem and funding the work throughout the ESGI and for their collaboration during and after the study group was held. The views expressed in this article are those of the authors and do not necessarily reflect the position or policy of PepsiCo, Inc. Kris Kiradjiev, Thomas Babb, and Raquel Gonzalez-Farina would also like to acknowledge the support of EPSRC Center for Doctoral Training in Industrially Focused Mathematical Modelling (EP/L015803/1).

REFERENCES

[1] S. Bakalis, K. Knoerzer, and P. J. Fryer, editors, *Modeling Food Processing Operations*, Woodhead Publishing, 2015.

[2] S. I. Barry and J. Caunce, *Exact and numerical solutions to a Stefan problem with two moving boundaries*, Appl. Math. Model., 32 (2008), pp. 83–98.

Copyright © by SIAM. Unauthorized reproduction of this article is prohibited.

[3] G. P. Benham, K. Hildal, C. P. Please, and R. A. Van Gorder, *Solidification of silicon in a one-dimensional slab and a two-dimensional wedge*, Int. J. Heat Mass Trans., 98 (2016), pp. 530–540.
[4] S. J. Board and R. W. Hall, *Recent advances in understanding large scale vapour explosions*, in Proceedings of the Third Specialist Meeting on Sodium Fuel Interactions in Fast Reactors, Tokyo, March, 1976.
[5] P. Bouchon, P. Hollins, M. Pearson, D. L. Pyle, and M. J. Tobin, *Oil distribution in fried potatoes monitored by infrared microspectroscopy*, J. Food Sci., 66 (2001), pp. 918–923.
[6] Y. Chen and R. G. Moreira, *Modelling of a batch deep-fat frying process for tortilla chips*, Food Bioproducts Process., 75 (1997), pp. 181–190.
[7] V. K. Dhir, *Viscous hydrodynamic instability theory of the peak and minimum pool boiling heat fluxes*, in College of Engineering, University of Kentucky, UKY BU100, 1972.
[8] A. Halder, A. Dhall, and A. K. Datta, *An improved, easily implementable, porous media based model for deep-fat frying: Part* i*: Model development and input parameters*, Food Bioproducts Process., 85 (2007), pp. 209–219.
[9] S. D. Howison, *Similarity solutions to the stefan problem and the binary alloy problem*, IMA J. Appl. Math., 40 (1988), pp. 147–161.
[10] M. L. Kawas and R. G. Moreira, *Characterization of product quality attributes of tortilla chips during the frying process*, J. Food Engrg., 47 (2001), pp. 97–107.
[11] K. B. Kiradjiev, S. A. Halvorsen, R. A. Van Gorder, and S. D. Howison, *Maxwell-type models for the effective thermal conductivity of a porous material with radiative transfer in the voids*, Int. J. Thermal Sci., 145 (2019).
[12] B. Louro and J. F. Rodrigues, *Remarks on the quasi-steady one phase Stefan problem*, Proc. Roy. Soc. Edinburgh Sect. A Math., 102 (1986), pp. 263–275.
[13] R. G. Moreira, *Deep-fat frying*, in WIT Transactions on State of the Art in Science and Engineering, vol. 13, WIT Press, 2007.
[14] R. G. Moreira and M. A. Barrufet, *A new approach to describe oil absorption in fried foods: A simulation study*, J. Food Engrg., 35 (1998), pp. 1–22.
[15] R. G. Moreira, X. Sun, and Y. Chen, *Factors affecting oil uptake in tortilla chips in deep-fat frying*, J. Food Engrg., 31 (1997), pp. 485–498.
[16] P. C. Moyano and F. Pedreschi, *Kinetics of oil uptake during frying of potato slices: Effect of pre-treatments*, LWT-Food Science and Technology, 39 (2006), pp. 285–291.
[17] T. G. Myers, M. G. Hennessy, and M. Calvo-Schwarzwälder, *The Stefan problem with variable thermophysical properties and phase change temperature*, preprint, arXiv:1904.05698, 2019.
[18] V. Voller and M. Cross, *Accurate solutions of moving boundary problems using the enthalpy method*, Int. J. Heat Mass Trans., 24 (1981), pp. 545–556.
[19] M. G. Worster, G. K. Batchelor, and H. K. Moffatt, *Solidification of fluids*, Perspectives in Fluid Dynamics, 742 (2000), pp. 393–446.
[20] R. Yamsaengsung and R. G. Moreira, *Modeling the transport phenomena and structural changes during deep fat frying: Part* i*: Model development*, J. Food Engrg., 53 (2002), pp. 1–10.
[21] A. M. Ziaiifar, N. Achir, F. Courtois, I. Trezzani, and G. Trystram, *Review of mechanisms, conditions, and factors involved in the oil uptake phenomenon during the deep-fat frying process*, Int. J. Food Sci. Tech., 43 (2008), pp. 1410–1423.

Downloaded 05/01/21 to 131.111.184.3. Redistribution subject to SIAM license or copyright; see https://epubs.siam.org/page/terms

Copyright © by SIAM. Unauthorized reproduction of this article is prohibited.